JOURNAL OF AIRCRAFT
Vol. 46, No. 2, March–April 2009

# Supersonic Flutter of Functionally Graded Panels Subject to Acoustic and Thermal Loads

Hesham Hamed Ibrahim,* Hong Hee Yoo,† and Kwan-Soo Lee‡
*Hanyang University, Seoul 133-791, Republic of Korea*

DOI: 10.2514/1.39085

**A nonlinear finite element model is provided for the supersonic flutter behavior of functionally graded material panels subject to combined aerodynamic, thermal, and random acoustic loads. Material properties are assumed to be temperature dependent and graded in the thickness direction according to a simple power law distribution in terms of the volume fractions of the constituents. The governing equations are derived using the classical plate theory with von Kármán geometric nonlinearity and the principle of virtual work. The first-order piston theory is adopted to model aerodynamic pressures induced by supersonic airflows. The thermal load is assumed to be steady-state constant temperature distribution, and the acoustic excitation is considered to be a stationary white-Gaussian random pressure with zero mean and uniform magnitude over the plate surface. The governing equations are transformed to modal coordinates to reduce the computational efforts. The Newton–Raphson iteration method is employed to obtain the dynamic response at each time step of the Newmark scheme for numerical integration. Finally, numerical results are provided to study the effects of the volume fraction exponent, aerodynamic pressure, temperature rise, and the random acoustic load on the panel response.**

## I. Introduction

FUNCTIONALLY graded materials (FGMs) are nonhomogeneous composites characterized by a smooth and continuous change of material properties from one surface to the other. This is achieved by gradually varying the volume fraction of the constituent materials. Functionally graded materials are usually composed of two or more materials whose volume fractions are changing smoothly and continuously along desired direction(s). This continuous change in the compositions leads to a smooth change in the mechanical properties, which has many advantages over the laminated composites, where the delamination and cracks are most likely to initiate at the interfaces due to the abrupt variation in the mechanical properties between laminas. One of the advantages of using these materials is that they can survive environments with high temperature gradients, while maintaining structural integrity. Accordingly, one of the most important applications of functionally graded materials is in the skin panels of supersonic and hypersonic flight vehicles, which have to survive the harsh thermal and mechanical loadings.

Thin plates are a commonly used form of structural components especially in aerospace vehicles, such as high-speed aircraft, rockets, and spacecrafts, which are subjected to aerodynamic loads, thermal loads due to aerodynamic and/or solar radiation heating, and random acoustic loads due to engine and/or aerodynamic transonic noise. This results in temperature and pressure distributions over the panel surface. The presence of these thermal and pressure fields results in a flutter motion at a lower aerodynamic pressure, or a larger flutter limit-cycle amplitude at the same aerodynamic pressure. In addition, a high temperature rise may cause large thermal deflections (thermal buckling) of the skin panels, which could affect flutter response. Accordingly, it is important to consider the interactive effect of aerodynamic, thermal, and random acoustic loads.

Panel flutter is a phenomenon that is usually accompanied by temperature elevation on the outer skin of high-speed air vehicles. Panel flutter is a self-excited oscillation of a plate or shell in supersonic flow. Because of aerodynamic pressure forces on the panel, two eigenmodes of the structure merge and lead to this dynamic instability. Panel flutter differs from wing flutter only in that the aerodynamic force resulting from the airflow acts only on one side of the panel. Most flutter analyses can be placed in one of four categories based on the structural and aerodynamic theories employed: 1) linear structural theory, quasi-steady aerodynamic theory; 2) linear structural theory, full linearized (inviscid, potential) aerodynamic theory; 3) nonlinear structural theory, quasi-steady aerodynamic theory; and 4) nonlinear structural theory, linearized (inviscid, potential) aerodynamic theory. Analyses of the first type have two major weaknesses: a) it does not account for structural nonlinearities, hence it can only determine the flutter boundary and can give no information about the flutter amplitudes; and b) the use of quasi-steady aerodynamics neglects the three dimensionality and unsteadiness of the flow, hence it cannot be used in the transonic region where the flutter is most likely to occur. Analyses of the second type are intended to remedy weakness b but this type still has weakness a. The third type remedies weakness a, but still posseses weakness b. The fourth type remedies both a and b [1].

Extensive research work has been carried out on the FGM since its concept was proposed in the late 1980s. Reddy [2] developed both theoretical and finite element formulations for thick FGM plates according to the higher order shear deformation plate theory, and studied the nonlinear dynamic response of FGM plates subjected to a suddenly applied uniform pressure. El-Abbasi and Meguid [3] provided a new thick shallow shell element to study the thermoelastic behavior of functionally graded structures made of shells and plates. The element accounts for the varying elastic and thermal properties across its thickness. Zenkour [4] presented a new generalized shear deformation theory to study the static response for a simply supported functionally graded rectangular plate subjected to a transverse uniform load. Dai et al. [5] developed a mesh free model for the active shape control and the dynamic response suppression of a functionally graded material plate containing piezoelectric sensors and actuators. He et al. [6] presented the vibration control of FGM thin plates with integrated piezoelectric sensors and actuators. Yang et al. [7] investigated the geometrically nonlinear bending behavior of FGM plates with integrated piezoelectric layers and subjected to

Received 13 June 2008; revision received 10 October 2008; accepted for publication 16 December 2008. 

*Assistant Professor, Department of Mechanical Engineering; currently National Authority for Remote Sensing and Space Sciences, Cairo, 11769, Egypt; hhibrahim76@hotmail.com.

†Professor, Department of Mechanical Engineering; hhyoo@hanyang.ac.kr.

‡Professor, Department of Mechanical Engineering; ksleehy@hanyang.ac.kr.

transverse loads and a temperature gradient through the plate thickness. Batra and Jin [8] adopted the first-order shear deformation theory coupled with a finite element method to study the vibration of a functionally graded anisotropic rectangular plate with different edge support conditions. The functional grading was achieved through continuously changing the fiber orientation angle through the thickness. Kim [9] developed an analytical technique to investigate the effect of temperature on the vibration characteristics of thick functionally graded rectangular plates, taking into account the temperature dependence of the material properties. However, the studies pertaining to flutter instability of FGM panels are rather sparsely treated in the literature compared to vibration analysis. The influence of thermal environment on the critical flutter dynamic pressure of a flat FGM panel was studied by Prakash and Ganapathi [10]. Navazi and Haddadpour [11] provided an analytical formulation to determine the aerothermoelastic stability margins of FGM panels. The effect of compressive in-plane loads and both uniform and through the thickness nonlinear temperature distributions were considered in their formulation. Haddadpour et al. [12] extended the work presented in [11] by studying the effect of the constituents volume fraction exponent on the flutter limit-cycle oscillation amplitudes of semi-infinite FGM plates. Ibrahim et al. [13] investigated the thermal buckling and flutter boundaries of thin FGM panels at elevated temperature. They adopted an incremental finite element technique to capture the effect of the temperature dependence of material properties on the panel response. Ibrahim et al. [14] developed a frequency-domain solution to predict the flutter limit-cycle oscillation amplitudes of thin FGM panels under combined aerodynamic and thermal loads. To account for the temperature dependence of material properties, the thermal strain was modeled as an integral quantity of a thermal expansion coefficient with respect to temperature. Ibrahim et al. [15] extended the formulation presented in [14] by including the shear deformation effect to make it capable of handling thick FGM panels. Sohn and Kim [16] studied the static and dynamic stabilities of FGM panels under supersonic airflows and elevated temperature environment, while assuming temperature-independent material properties. However, to the best of the authors' knowledge, the combined effect of aerodynamic, thermal, and acoustic loads on the flutter limit-cycle oscillation of FGM panels has not yet been accomplished in the literature. As the use of panels made of functionally graded materials is expected to increase, it is worth investigating the nonlinear response of such panels under combined aerodynamic, thermal, and random acoustic loads.

In this work, a time-domain solution is presented for the nonlinear flutter response of clamped FGM panels under combined aerodynamic, thermal, and random acoustic loads. A nonlinear finite element model is provided based on the classical plate theory with von Kármán geometric nonlinearity and the principle of virtual work. Material properties are assumed to be temperature dependent and graded in the thickness direction according to a simple power law distribution in terms of the volume fractions of the constituents. Finally, numerical results are provided to study the effects of volume fraction exponent, aerodynamic pressure, temperature rise, and random acoustic load on the panel response.

## II. Finite Element Formulation

The equation of motion with the consideration of large deflection and temperature dependence of material properties are derived for a functionally graded plate subject to aerodynamic, thermal, and random acoustic loads. To account for temperature dependence of material properties, the thermal strain is modeled as an integral quantity of the thermal expansion coefficient. The element used in this study is the rectangular four-node Bogner–Fox–Schmidt $C^1$ conforming element (for the bending degrees of freedom) [17].

### A. Nonlinear Strain-Displacement Relations

The nodal degrees of freedom vector $\{\theta\}$ of the rectangular plate element having 6 degrees of freedom at each nose can be written as

$$\{\theta\} = \left\{\left\{w, \frac{\partial w}{\partial x}, \frac{\partial w}{\partial y}, \frac{\partial^2 w}{\partial x \partial y}\right\}, \{u, v\}\right\}^T = \begin{Bmatrix} \{w_b\} \\ \{w_m\} \end{Bmatrix} \tag{1}$$

where $\{w_b\}$ is the transverse displacement vector and $\{w_m\}$ is the membrane displacement vector. In-plane strains and curvatures, based on von Kármán moderately large deflection and classical thin plate theory, are given by

$$\begin{Bmatrix} \varepsilon_x \\ \varepsilon_y \\ \gamma_{xy} \end{Bmatrix} = \begin{Bmatrix} \frac{\partial u}{\partial x} \\ \frac{\partial v}{\partial y} \\ \frac{\partial u}{\partial y} + \frac{\partial v}{\partial x} \end{Bmatrix} + \begin{Bmatrix} \frac{1}{2}\left(\frac{\partial w}{\partial x}\right)^2 \\ \frac{1}{2}\left(\frac{\partial w}{\partial y}\right)^2 \\ \frac{\partial w}{\partial x}\frac{\partial w}{\partial y} \end{Bmatrix} + z \begin{Bmatrix} -\frac{\partial^2 w}{\partial x^2} \\ -\frac{\partial^2 w}{\partial y^2} \\ -2\frac{\partial^2 w}{\partial x \partial y} \end{Bmatrix}$$
$$= \{\varepsilon_m\} + \{\varepsilon_\theta\} + z\{\kappa\} \tag{2}$$

Parameters $u$, $v$, and $w$ are displacements in the $x$, $y$, and $z$ directions, respectively. $\varepsilon_m$, $\varepsilon_\theta$, and $z\kappa$ are the membrane linear strain vector, the membrane nonlinear strain vector, and the bending strain vector, respectively.

### B. Functionally Graded Materials

Typically, the FGMs are made of a mixture of two materials: a ceramic, which is capable of withstanding high temperature environments due to its low thermal conductivity, and a metal which acts as a structural element to support loading and prevent fractures. Without losing generality, it is usually assumed that the top surface of an FGM plate is ceramic rich and the bottom is metal rich. The region between the two surfaces consists of a blend of the two materials which is assumed in the form of a simple power law distribution as [5]

$$P_e(z) = P_C V_C + P_M(1 - V_C) \tag{3}$$

$$V_C = \left(0.5 + \frac{z}{h}\right)^n, \qquad (-h/2 \le z \le h/2, 0 \le n \le \infty) \tag{4}$$

where $z$ is the coordinate in the thickness direction of a plate; $(P_e, P_c, P_M)$ are effective material properties of the FGM, the properties of the ceramic and the properties of the metal, respectively. $V_c$ is the ceramic volume fraction, $h$ is the panel thickness, and power $n$ is the volume fraction exponent. Figure 1 shows the variation of the volume fraction function, $n$, versus the nondimensional thickness, $z/h$, with different volume fraction exponent $n$.

### C. Stress–Strain Relationship of an FGM Panel

The relationship of in-plane forces $\{N\}$ and bending moments $\{M\}$ in terms of the strain vectors can be written as

$$\{N\} = [A]\{\varepsilon_m + \varepsilon_\theta\} + [B]\{\kappa\} - \{N_T\} \tag{5}$$

$$\{M\} = [B]\{\varepsilon_m + \varepsilon_\theta\} + [D]\{\kappa\} - \{M_T\} \tag{6}$$

where

$$([A], [B], [D]) = \int_{-h/2}^{h/2} (1, z, z^2)[Q(z, T, n)]\mathrm{d}z$$

$$[Q(z, T, n)] = \begin{bmatrix} \frac{E(z,T,n)}{1-\nu^2(z,n)} & \frac{\nu E(z,T,n)}{1-\nu^2(z,n)} & 0 \\ \frac{\nu E(z,T,n)}{1-\nu^2(z,n)} & \frac{E(z,T,n)}{1-\nu^2(z,n)} & 0 \\ 0 & 0 & \frac{E(z,T,n)}{2(1+\nu(z,n))} \end{bmatrix}$$

$$\begin{Bmatrix} N_T \\ M_T \end{Bmatrix} = \int_{-h/2}^{h/2} \left[\left(\int_{T_{\mathrm{ref}}}^{T} [Q(z, \tau, n)]\{\alpha(z, \tau, n)\}\mathrm{d}\tau\right)\right] \begin{Bmatrix} 1 \\ z \end{Bmatrix} \mathrm{d}z$$

where $[A]$, $[B]$, and $[D]$ are the extensional stiffness matrix, the extensional-bending coupling stiffness matrix, and the flexural stiffness matrix, respectively. $T$ denotes the temperature, while

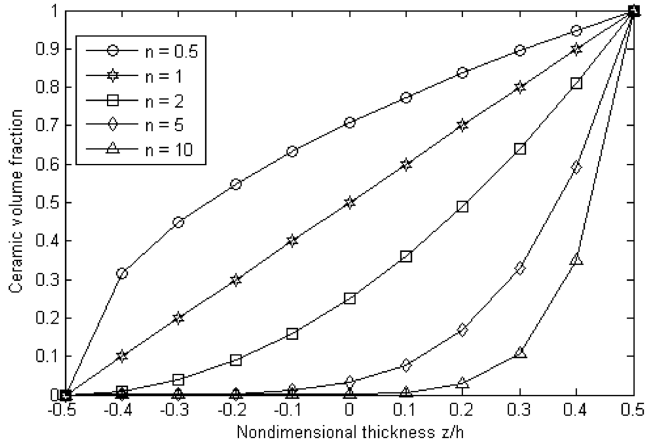


**Fig. 1 Variation of the ceramic volume fraction function versus the nondimensional thickness $z/h$.**

constant temperature distributions in the $x$, $y$, and $z$ directions are assumed. In addition, $\alpha$ denotes the thermal expansion coefficient.

### D. Aerodynamic Loading

The aerodynamic pressure caused by a supersonic airflow will be approximated by the first-order quasi-steady piston theory, which is valid for $\sqrt{2} < M_\infty$ and shows good accuracy in the range of $\sqrt{2} < M_\infty < 5$. The aerodynamic pressure using the first-order piston theory is expressed as [14]

$$P_a = -\left(\frac{g_a}{\omega_o}\frac{D_{11}}{a^4}\frac{\partial w}{\partial t} + \lambda\frac{D_{11}}{a^3}\frac{\partial w}{\partial x}\right) \tag{7}$$

with

$$g_a = \sqrt{\lambda C_a},\ C_a = \frac{(M_\infty^2-2)^2}{(M_\infty^2-1)^2}\frac{\rho_a a}{\rho h \beta},\qquad \lambda = \frac{2qa^3}{\beta D_{11}}$$

$$q = \frac{\rho_a V^2}{2},\qquad \beta = \sqrt{M_\infty^2-1},\quad \text{and}\quad \omega_o = \left(\frac{D_{11}}{\rho h a^4}\right)^{\frac{1}{2}}$$

where $P_a$ is the aerodynamic pressure loading, $V$ is the airflow velocity on one side of the panel, $M_\infty$ is the Mach number, $q$ is the dynamic pressure, $\rho$ and $\rho_a$ are the panel and air mass densities, respectively, $g_a$ is the nondimensional aerodynamic damping, $C_a$ is the aerodynamic damping coefficient, $\lambda$ is the nondimensional dynamic pressure, $D_{11}$ is the first entry in the flexural stiffness matrix $D(1,1)$, and $a$ is the streamwise panel length.

### E. Acoustic Load Simulation

The acoustic excitation is assumed as a stationary white-Gaussian random pressure with zero mean and uniform magnitude over the panel surface. Noting that, for the finite element time-domain integration method presented in this study, there is no limitation on the random input excitation. It can be stationary or nonstationary and Gaussian or non-Gaussian, as long as a time history for the random excitation is available. The cross-spectrum density $S_p$ of a truncated white-Gaussian pressure uniformly distributed over the panel surface can be given as [18]

$$S_p = \begin{cases} S_0 = p_0^2 10^{\mathrm{SPL}/10}, & 0 \le f \le f_u \\ 0, & f < 0 \quad \text{or} \quad f > f_u \end{cases} \tag{8}$$

where $S_o$ is a constant, $p_0$ is a reference pressure, $p_0 = 20\ \mu$Pa, SPL is the sound pressure level in decibels, and $f_u$ is the upper cutoff frequency in Hz. Using MATLAB, the Gaussian random pressure $p(t)$ with zero mean and power $PW$ is expressed as

$$p(t) = \sqrt{(PW)} \cdot randn([n, 1]) \tag{9}$$

where $randn$ is a Gaussian random number generation function, and $n$ is the amount of numbers need to be generated. For numerical integration, it is equal to the time duration divided by the time step. The power can be calculated from spectrum density $S_0$ and upper cutoff frequency $f_u$ as

$$PW = S_0 \cdot f_u \tag{10}$$

The cutoff frequency should be selected so that it does not only cover the highest natural frequency in the simulation, but also considers the frequency shifting effect due to the nonlinear large amplitude vibration. Generally speaking, it should be selected at least twice the highest linear frequency of the modes included in the simulation.

### F. Governing Equations

By using the principle of virtual work and Eqs. (2), (5), and (6), the governing equation can be derived as follows:

$$\delta W = \delta W_{\text{int}} - \delta W_{\text{ext}} = 0 \tag{11}$$

The internal virtual work $\delta W_{\text{int}}$ is given as

$$\begin{aligned}\delta W_{\text{int}} &= \int_A (\{\delta\varepsilon_m\}^T\{N\} + \{\delta\kappa\}^T\{M\})\mathrm{d}A \\ &= \{\delta\theta\}^T\left([k] - [k_T] + \frac{1}{2}[n1] + \frac{1}{3}[n2]\right)\{\theta\} - \{\delta\theta\}^T\{p_T\}\end{aligned} \tag{12}$$

where $\{\theta\} = [\,w \quad w_x \quad w_y \quad w_{xy} \quad u \quad v\,]$ is the nodal displacement vector; $[k]$ and $[k_T]$ are the linear stiffness matrix and the thermal geometric stiffness matrix, respectively; and $[n1]$ and $[n2]$ are the first- and second-order nonlinear stiffness matrices, respectively [19]. In addition, $\{p_T\}$ is the thermal load vector. On the other hand, the virtual work done by external forces on a plate element, considering inertia and random pressure excitations, is

$$\begin{aligned}\delta W_{\text{ext}} = \int_A (&\delta w(-\rho h\ddot{w} + P_a + p(t)) \\ &+ \delta u(-\rho h\ddot{u}) + \delta v(-\rho h\ddot{v}))\mathrm{d}A\end{aligned} \tag{13}$$

where $p(t)$ represents the acoustic load which is modeled as a white-Gaussian random pressure. The virtual work of aerodynamic loading, $P_a$, using the quasi-steady first-order piston theory can be written as [15]

$$\begin{aligned}\int_A \delta w P_a \mathrm{d}A &= -\int_A \delta w\left(\frac{g_a}{\omega_0}\frac{D_{11}}{a^4}\frac{\partial w}{\partial t} + \lambda\frac{D_{11}}{a^3}\frac{\partial w}{\partial x}\right)\mathrm{d}A \\ &= -\{\delta w_b\}^T[g_a]\{\dot{w}_b\} - \{\delta w_b\}^T\lambda[a_a]\{w_b\}\end{aligned} \tag{14}$$

The finite element form of the virtual work done by inertia and aerodynamic forces on a plate element takes the form:

$$\begin{aligned}\delta W_{\text{ext}} = &-\begin{Bmatrix}\{\delta w_b\}\\ \{\delta w_m\}\end{Bmatrix}^T\begin{bmatrix}[m_b] & 0\\ 0 & [m_m]\end{bmatrix}\begin{Bmatrix}\{\ddot{w}_b\}\\ \{\ddot{w}_m\}\end{Bmatrix} \\ &-\begin{Bmatrix}\{\delta w_b\}\\ \{\delta w_m\}\end{Bmatrix}^T\begin{bmatrix}[g_a] & 0\\ 0 & 0\end{bmatrix}\begin{Bmatrix}\{\dot{w}_b\}\\ \{\dot{w}_m\}\end{Bmatrix} \\ &-\lambda\begin{Bmatrix}\{\delta w_b\}\\ \{\delta w_m\}\end{Bmatrix}^T\begin{bmatrix}[a_a] & 0\\ 0 & 0\end{bmatrix}\begin{Bmatrix}\{w_b\}\\ \{w_m\}\end{Bmatrix} + \begin{Bmatrix}\{\delta w_b\}\\ \{\delta w_m\}\end{Bmatrix}^T\begin{Bmatrix}\{p_b(t)\}\\ 0\end{Bmatrix}\end{aligned} \tag{15}$$

where $[m_b]$ and $[m_m]$ are bending and in-plane inertia matrices, respectively. $[g_a]$ is the aerodynamic damping matrix, and $[a_a]$ is the aerodynamic stiffness matrix. Combining Eqs. (12) and (15), the element equation of motion is expressed as

$$\begin{aligned}&[m]\{\ddot{\theta}\} + [\bar{g}]\{\dot{\theta}\} + (\lambda[\bar{a}_a] + [k] - [k_T] + \tfrac{1}{2}[n1] + \tfrac{1}{3}[n2])\{\theta\} \\ &\quad = \{p(t)\} + \{p_T\}\end{aligned} \tag{16}$$

Assembling the element equations of motion to the system level by summing up the contributions from all elements and applying the boundary conditions, the system equations of motion become

$$[M]\{\ddot{W}\} + [G]\{\dot{W}\} + (\lambda[A] + [K] - [K_T] + \tfrac{1}{2}[N1] + \tfrac{1}{3}[N2])\{W\} = \{P(t)\} + \{P_T\} \quad (17)$$

## III. Solution Procedures

In this section, a time-domain solution is presented for the nonlinear flutter response of FGM panels under combined aerodynamic, thermal, and random acoustic loads. Equation (17) can be stated as

$$\begin{bmatrix} [M_b] & 0 \\ 0 & [M_m] \end{bmatrix} \begin{Bmatrix} \{\ddot{W}_b\} \\ \{\ddot{W}_m\} \end{Bmatrix} + \begin{bmatrix} [G_a] & 0 \\ 0 & 0 \end{bmatrix} \begin{Bmatrix} \{\dot{W}_b\} \\ \{\dot{W}_m\} \end{Bmatrix} + \left( \lambda \begin{bmatrix} [A_a] & 0 \\ 0 & 0 \end{bmatrix} + \begin{bmatrix} [K_b] & [K_{bm}] \\ [K_{mb}] & [K_m] \end{bmatrix} - \begin{bmatrix} [K_{Tb}] & 0 \\ 0 & 0 \end{bmatrix} + \frac{1}{2} \begin{bmatrix} [N1_{Nm}(\{W_m\}) + N1_{Nb}(\{W_b\})] & [N1_{bm}] \\ [N1_{mb}] & 0 \end{bmatrix} + \frac{1}{3} \begin{bmatrix} [N2_b] & 0 \\ 0 & 0 \end{bmatrix} \right) \begin{Bmatrix} \{W_b\} \\ \{W_m\} \end{Bmatrix} = \begin{Bmatrix} \{P_b(t)\} \\ 0 \end{Bmatrix} + \begin{Bmatrix} \{P_{Tb}\} \\ \{P_{Tm}\} \end{Bmatrix} \quad (18)$$

where the subscripts $m$ and $b$ denote membrane and bending, respectively. Separating the membrane and transverse displacement equations in Eq. (18):

$$[M_b]\{\ddot{W}_b\} + [G_a]\{\dot{W}_b\} + (\lambda[A_a] + [K_b] - [K_{Tb}] + \tfrac{1}{2}[N1_{Nm}(\{W_m\})] + \tfrac{1}{2}[N1_{Nb}(\{W_b\})] + \tfrac{1}{3}[N2_b])\{W_b\} + ([K_{bm}] + \tfrac{1}{2}[N1_{bm}])\{W_m\} = \{P_b(t)\} + \{P_{Tb}\} \quad (19)$$

$$[M_m]\{\ddot{W}_m\} + ([K_{mb}] + \tfrac{1}{2}[N1_{mb}])\{W_b\} + [K_m]\{W_m\} = \{P_{Tm}\} \quad (20)$$

Note that, neglecting the in-plane inertia term will not bring significant error because the in-plane natural frequencies are 2 to 3 orders of magnitude higher than the bending ones [20]. Therefore, the in-plane displacement can be expressed in terms of the bending displacement as

$$\begin{aligned} \{W_m\} &= [K_m]^{-1}(\{P_{Tm}\} - ([K_{mb}] + \tfrac{1}{2}[N1_{mb}])\{W_b\}) \\ &= [K_m]^{-1}\{P_{Tm}\} - [K_m]^{-1}[K_{mb}]\{W_b\} - \tfrac{1}{2}[K_m]^{-1}[N1_{mb}]\{W_b\} \\ &= \{W_m\}_0 - \{W_m\}_1 - \{W_m\}_2 \end{aligned} \quad (21)$$

It can be shown that [19]

$$\tfrac{1}{2}[N1_{bm}]\{W_m\}_0 = \tfrac{1}{2}[N1_{Nm}(\{W_m\}_0)]\{W_b\} \quad (22)$$

Accordingly, by substituting Eq. (21) into (19), Eq. (19) can be written as

$$\begin{aligned} &[M_b]\{\ddot{W}_b\} + [G_a]\{\dot{W}_b\} + (\lambda[A_a] + [K_b] - [K_{Tb}] \\ &\quad - [K_{bm}][K_m]^{-1}[K_{mb}] + [N1_{Nm}(\{W_m\}_0)] + \tfrac{1}{2}[N1_{Nb}] \\ &\quad - \tfrac{1}{2}[N1_{Nm}(\{W_m\}_1)] - \tfrac{1}{2}[N1_{bm}][K_m]^{-1}[K_{mb}] \\ &\quad - \tfrac{1}{2}[K_{bm}][K_m]^{-1}[N1_{mb}] + \tfrac{1}{3}[N2_b] - \tfrac{1}{4}[N1_{bm}][K_m]^{-1}[N1_{mb}] \\ &\quad - \tfrac{1}{2}[N1_{Nm}(\{W_m\}_2)])\{W_b\} \\ &\quad = \{P_b(t)\} + \{P_{Tb}\} - [K_{bm}][K_m]^{-1}\{P_{Tm}\} = \{P_B\} \end{aligned} \quad (23)$$

An effective solution procedure is to transform Eq. (23) into modal coordinates using reduced system normal modes by expressing the system bending displacement $\{W_b\}$ as a linear combination of some mode shapes as

$$\{W_b\} \approx \sum_{r=1}^{n} Q_r\{\phi_r\} = [\Phi]\{Q\} \quad (24)$$

where the $r$th normal mode $\{\phi_r\}$ and the corresponding natural frequency $\omega_r$ are obtained from the linear vibration of the system as

$$\omega_r^2[M_b]\{\phi_r\} = ([K_b] - [K_{bm}][K_m]^{-1}[K_{mb}])\{\phi_r\} \quad (25)$$

Based on the normal modes evaluated in Eq. (25), all the matrices in Eq. (23) are transformed into modal coordinates. Accordingly, Eq. (23) can be written in modal coordinates as

$$[\bar{M}_b]\{\ddot{Q}\} + (2[\zeta_r\omega_r][\bar{M}_b] + [\bar{G}])\{\dot{Q}\} + ([\bar{K}] + [\bar{K}_q] + [\bar{K}_{qq}])\{Q\} = \{\bar{P}_B\} \quad (26)$$

where the modal mass and modal linear stiffness matrices are given by

$$([\bar{M}_b], [\bar{G}], [\bar{K}]) = [\Phi]^T([M_b], [G_a], [K_{\text{lin}}])[\Phi] \quad (27)$$

and

$$[K_{\text{lin}}] = \lambda[A_a] + [K_b] - [K_{Tb}] - [K_{bm}][K_m]^{-1}[K_{mb}] + [N1_{Nm}(\{W_m\}_0)] \quad (28)$$

The first-order and second-order nonlinear modal stiffness matrices are given by

$$[\bar{K}_q] = [\Phi]^T \sum_{r=1}^{n} Q_r \left( \frac{1}{2}[N1_{Nb}]^{(r)} - \frac{1}{2}[N1_{Nm}(\{W_m\}_1)]^{(r)} - \frac{1}{2}[N1_{bm}]^{(r)}[K_m]^{-1}[K_{mb}] - \frac{1}{2}[K_{bm}][K_m]^{-1}[N1_{mb}]^{(r)} \right)[\Phi] \quad (29)$$

$$[\bar{K}_{qq}] = [\Phi]^T \sum_{r=1}^{n}\sum_{s=1}^{n} Q_r Q_s \left( \frac{1}{3}[N2_b]^{(rs)} - \frac{1}{2}[N1_{Nm}(\{W_m\}_2)]^{(rs)} - \frac{1}{4}[N1_{bm}]^{(r)}[K_m]^{-1}[N1_{mb}]^{(s)} \right)[\Phi] \quad (30)$$

$$\{\bar{P}_B\} = [\Phi]^T\{P_B\} \quad (31)$$

A modal structural damping matrix $2[\,\zeta_r \quad \omega_r\,][M_b]$ has been added to Eq. (26) to account for the structural damping effect on the system. The coefficient $\zeta_r$ is the modal damping ratio of the $r$th mode, while $\omega_r$ is the $r$th natural frequency in Hz [20].

## IV. Numerical Results and Discussions

The nonlinear vibration behavior of an FGM panel is investigated with four parameters in the study: volume fraction exponent $n$, temperature rise $\Delta T$, sound pressure level SPL, and nondimensional dynamic pressure $\lambda$. The panel is modeled using a $10 \times 10$ mesh. All panel edges are assumed clamped. A damping ratio that follows the relation $\zeta_r f_r = \zeta_s f_s$ is used with a fundamental modal damping coefficient $\zeta_1$ equal to 0.02. The aerodynamic damping coefficient $C_a$ is set to 0.1 [21]. The Newmark implicit numerical integration scheme is used to solve the system differential equations, while the Newton–Raphson iteration scheme is adopted to solve the nonlinear algebraic system of equations at each time step [22]. Modal transformation using nine normal modes was found giving a converged solution and thus used, noting that linear normal modes can efficiently express the panel nonlinear response in panels with all edges clamped [23]. The dimensions of the FGM panel are chosen to be $0.38 \times 0.305 \times 0.002$ m. A uniform temperature rise is applied to the plate, and the reference temperature is assumed to be 21°C. The FGM panel adopted in this study is a mixture of nickel and silicon nitride ($Si_3N_4$). The properties of the constituent materials are assumed to be temperature dependent according to the following relation:

**Table 1 Temperature-dependence coefficients for nickel and silicon nitride**

| Properties | Material | $P_{-1}$ | $P_0$ | $P_1$ | $P_2$ | $P_3$ |
|---|---|---|---|---|---|---|
| $E$, MPa | $Si_3N_4$ | 0 | 348.43e9 | −3.07e − 4 | 2.2e − 7 | −8.9e − 11 |
| | Nickel | 0 | 223.95e9 | −2.79e − 4 | 3.9e − 9 | 0 |
| $\nu$ | $Si_3N_4$ | 0 | 0.24 | 0 | 0 | 0 |
| | Nickel | 0 | 0.31 | 0 | 0 | 0 |
| $\alpha$ | $Si_3N_4$ | 0 | 5.8723e − 6 | 9.09e − 4 | 0 | 0 |
| | Nickel | 0 | 9.9209e − 6 | 8.71e − 4 | 0 | 0 |
| $\rho$, Kg/m$^3$ | $Si_3N_4$ | | | 2370 | | |
| | Nickel | | | 8900 | | |

$$P = P_0(P_{-1}T^{-1} + 1 + P_1T + P_2T^2 + P_3T^3) \tag{32}$$

where the coefficients $P_0$, $P_{-1}$, $P_1$, $P_2$, and $P_3$ for young's modulus $E$, the Poisson ratio $\nu$, and the thermal expansion coefficient $\alpha$ of nickel and silicon nitride are given in Table 1 [24].

### A. Validation of the Formulation

To validate the present formulation, flutter limit-cycle oscillation results were compared to those of Dowell [21]. The flutter limit-cycle oscillations for an aluminum square panel at two different values of the nondimensional dynamic pressure λ are presented in Fig. 2. The panel dimensions are $0.305 \times 0.305 \times 0.00127$ m with all edges simply supported. The aerodynamic damping coefficient $C_a$ is set to 0.1. Nine normal modes were used with a time step for numerical integration equal to $1/10,000$ s. The flutter limit-cycle amplitudes at $\lambda = 700$ and 800 were compared to those of Dowell [21] shown in Fig. 3, and good agreement is found between them.

### B. Nonlinear Vibration Behavior

The critical temperature boundary and linear flutter boundary of the nickel–silicon nitride FGM panel under the effect of thermal and aerodynamic loading are shown in Fig. 4, noting that this figure was provided before by Ibrahim et al. [15]. The area of the graph is divided into three regions: 1) the flat panel region, in which the panel is stable, that is, neither buckling nor panel flutter occurred; 2) the buckled region, in which the thermal stresses overcome the panel stiffness and aerodynamic stiffness (in this region, the panel undergoes static instability under in-plane thermal loading); and 3) the flutter region, where the panel undergoes dynamic instability under the influence of aerodynamic pressure. Thus, the wider the flat panel region is, the more stable the panel is. It is seen in Fig. 4 that decreasing the volume fraction exponent $n$ results in a wider flat panel region and in turn a more stable panel. It is worth noting that, for all simulation presented in this study, $D_{11}$ is evaluated at $T_{\text{ref}}$ and $n = \infty$ (i.e., $D_{11}$ is evaluated using the nickel properties at room temperature).

Time history responses for a panel at room temperature, $\lambda = 0$ and 700, SPL = 110 dB, and $n = 0$ ($Si_3N_4$), 1, and $\infty$ are presented in Figs. 5 and 6. For $\lambda = 0$, it is seen in Fig. 5 that the FGM panel (i.e., $n = 1$) has the highest rms value, whereas the ceramic panel has the highest time response frequency. Therefore, a fatigue analysis should be performed to point out which is a significant factor between the frequency and the deflection in such case. It is also noticed that the FGM panel response is not intermediate to those of the other two panels as was the case in the thermal buckling temperatures and the linear flutter boundaries shown in Fig. 4. Figure 6 illustrates the effect of the presence of an airflow with $\lambda = 700$, which is less than the flutter critical dynamic pressures for all the panels. It is seen that the airflow adds stiffness to the panels resulting in lower deflection rms values compared to those of Fig. 5.

Figures 7 and 8 present the time history responses with the same SPL and λ values presented in Figs. 5 and 6, but with a temperature rise value $\Delta T = 8$°C. Before the occurrence of thermal buckling, the nickel panel loses stiffness faster than the FGM and ceramic panels. Accordingly, the FGM and ceramic panels turned out to have a better performance than the nickel panel compared to the trend shown in

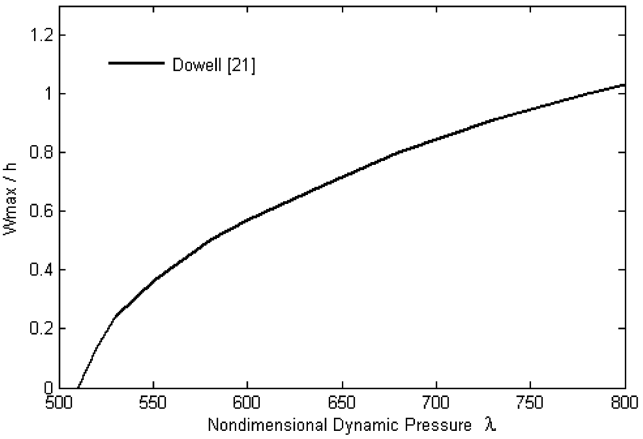


**Fig. 3 Flutter limit-cycle oscillation amplitudes versus λ for a simply supported aluminum square panel [21].**

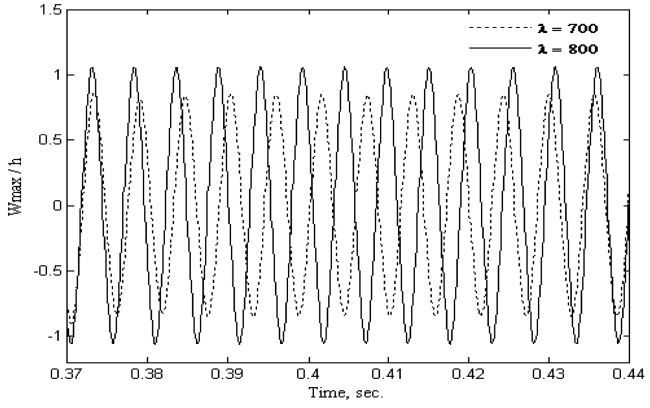


**Fig. 2 Flutter limit-cycle oscillation for a simply supported aluminum square panel at different nondimensional dynamic pressures, λ.**

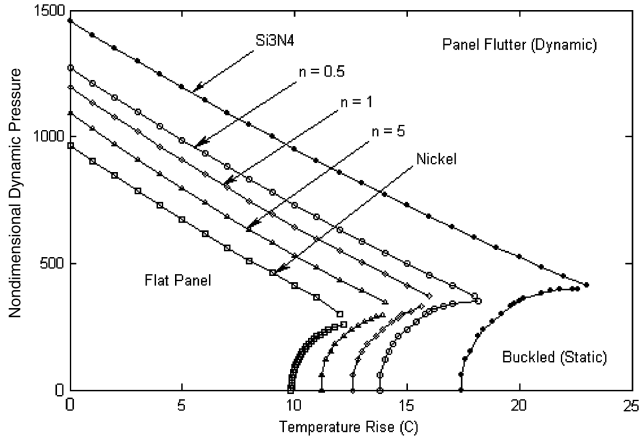


**Fig. 4 The effectiveness of the volume fraction exponent $n$ on the stability boundaries of an FGM clamped panel.**

Fig. 5. As the critical nondimensional dynamic pressure for the nickel panel is exceeded at $\lambda = 700$ and $\Delta T = 8°C$, it is seen in Fig. 8 that the nickel panel turned to flutter with harmonic limit-cycle oscillations with a vibration amplitude much larger than those of the FGM and ceramic panels. Accordingly, the FGM panels are found to have favorable performance compared to the nickel panels at $\Delta T = 8°C$. Moreover, it is also found that the presence of airflow is forcing the FGM panel response to be intermediate to those of nickel and ceramic.

At a temperature rise value $\Delta T = 16°C$, the critical buckling temperatures for both nickel and FGM panels are exceeded as shown in Fig. 4. Accordingly, due to the nonlinear stiffness added to the panels through having thermal postbuckling deflections, it is found in Fig. 9 that the nickel and FGM panels show small amplitude random vibrations about one of the two equilibrium buckling positions with the occurrence of a snap-through motion in the FGM panel at the beginning of the response. Therefore, it turns out to be a compromise between having higher thermal postbuckling deflections with smaller vibration amplitudes and hence more deterioration in the aerodynamic performance, as is the case of the nickel panel response, or having lower thermal postbuckling deflections with higher vibration amplitudes and hence a lower fatigue performance, as is the case of the FGM panel. Adding the effect of an airflow with $\lambda = 700$ along with a temperature rise of $\Delta T = 16°C$, it is found that all the flutter critical dynamic pressures are exceeded for all the panels, as shown in Fig. 4. Accordingly, it is seen in Fig. 10 that both nickel and FGM panels are fluttering with nearly harmonic limit-cycle

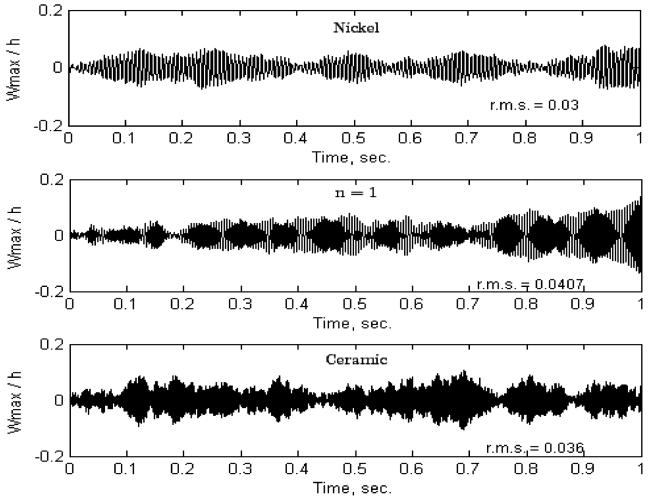


**Fig. 5 Time histories for an FGM panel at SPL = 110 dB, $\lambda = 0$, $\Delta T = 0°C$, and different volume fraction exponent values.**

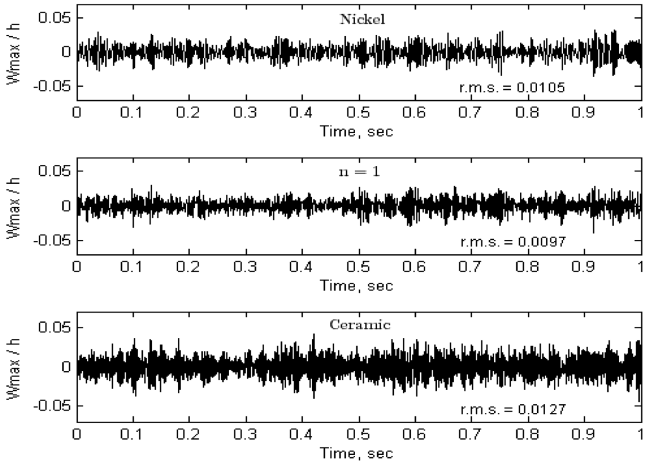


**Fig. 6 Time histories for an FGM panel at SPL = 110 dB, $\lambda = 700$, $\Delta T = 0°C$, and different volume fraction exponent values.**

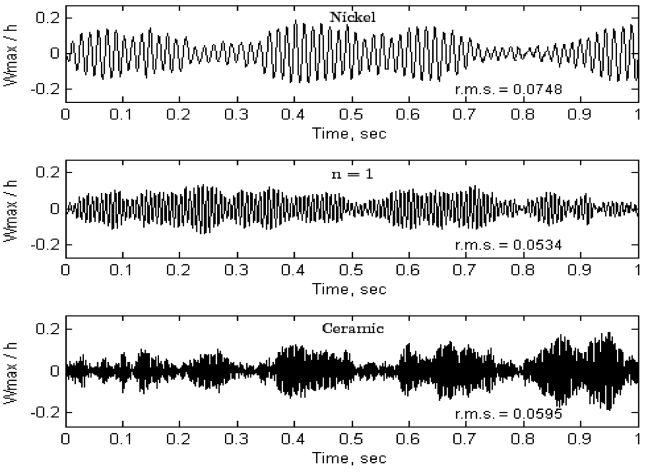


**Fig. 7 Time histories for an FGM panel at SPL = 110 dB, $\lambda = 0$, $\Delta T = 8°C$, and different volume fraction exponent values.**

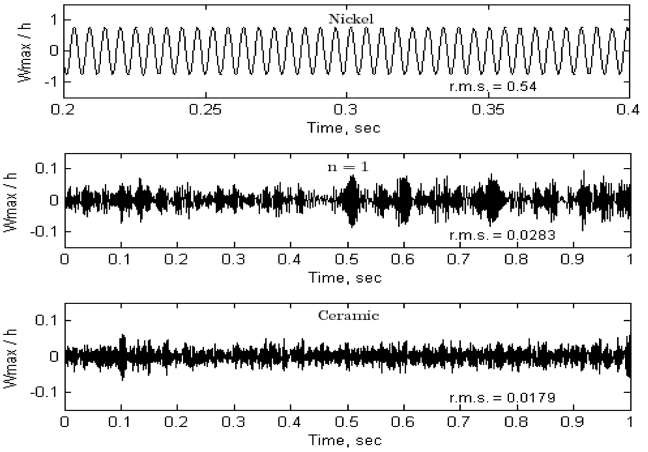


**Fig. 8 Time histories for an FGM panel at SPL = 110 dB, $\lambda = 700$, $\Delta T = 8°C$, and different volume fraction exponent values.**

oscillations, while the random acoustic response is still dominating the flutter motion in the ceramic panel. It is also noticed that the FGM panel shows a lower flutter limit-cycle oscillation amplitude with a higher frequency compared to the nickel panel. Therefore, in spite of the lower amplitudes of the FGM panels, the nickel panels may survive a longer time under these loads.

Figures 11 and 12 present the time history responses for $\Delta T = 24°C$ and $\lambda = 0$ and 700. It is seen in Fig. 11 that the ceramic plate has

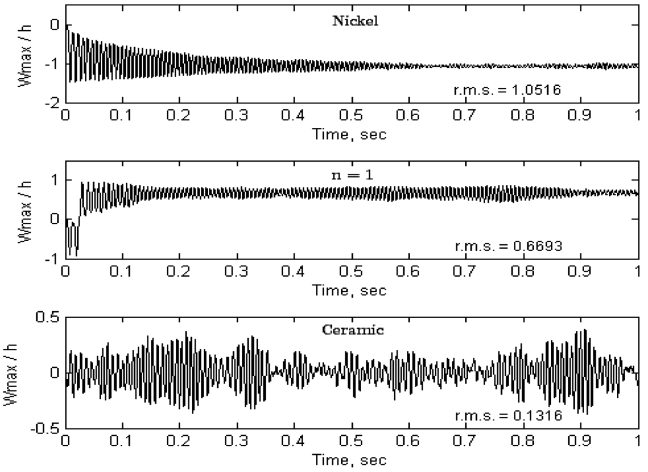


**Fig. 9 Time histories for an FGM panel at SPL = 110 dB, $\lambda = 0$, $\Delta T = 16°C$, and different volume fraction exponent values.**

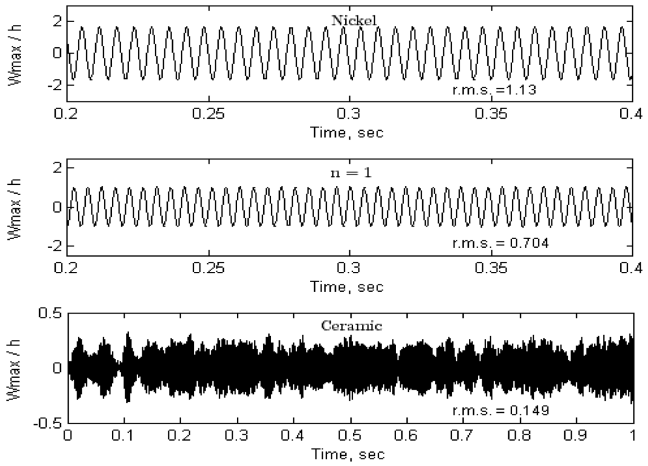


**Fig. 10 Time histories for an FGM panel at SPL = 110 dB, $\lambda = 700$, $\Delta T = 16°C$, and different volume fraction exponent values.**

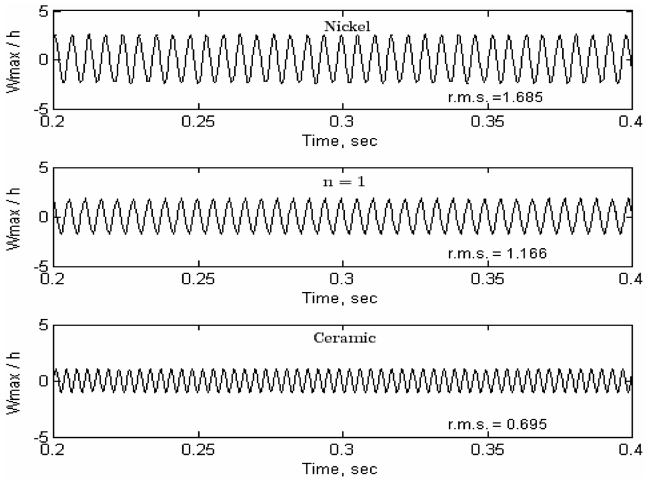


**Fig. 12 Time histories for an FGM panel at SPL = 110 dB, $\lambda = 700$, $\Delta T = 24°C$, and different volume fraction exponent values.**

the smallest thermal postbuckling deflection and the largest vibration amplitudes. Moreover, it can be concluded from Fig. 12 that, at high temperatures and dynamic pressures, decreasing the volume fraction exponent will always result in decreasing the limit-cycle oscillation amplitudes along with increasing the flutter frequency. Figure 13 illustrates the effect of increasing the SPL from 110 up to 130 dB. It is noticed that increasing the SPL has almost no quantitative effect on the flutter amplitude while having a noticeable qualitative effect on the flutter behavior through increasing the number of cycles flutter vibration and changing the type vibration to be nonharmonic or chaotic limit-cycle oscillations as shown in the phase plots of Fig. 13. So far, it is concluded that the existence of high sound pressure level values can noticeably affect the panel fatigue life performance.

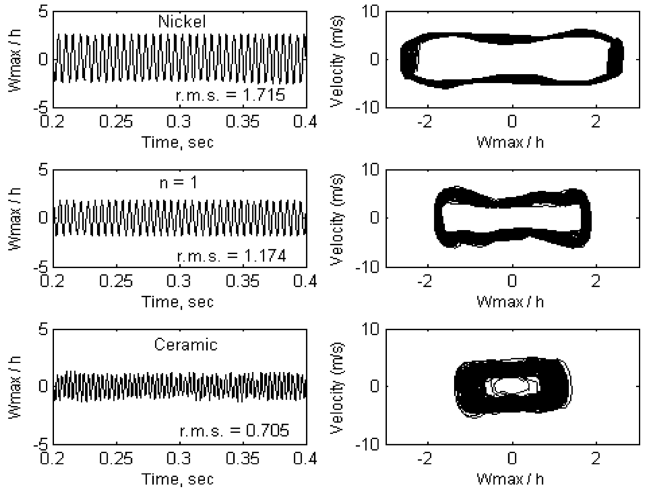


**Fig. 13 Time histories for an FGM panel at SPL = 130 dB, $\lambda = 700$, $\Delta T = 24°C$, and different volume fraction exponent values.**

## V. Conclusions

In this work, a time-domain solution is presented for the nonlinear flutter response of clamped FGM panels under combined aerodynamic, thermal, and random acoustic loads. A nonlinear finite element model is provided based on the classical plate theory with von Kármán geometric nonlinearity and the principle of virtual work. Material properties are assumed to be temperature dependent, and graded in the thickness direction according to a simple power law distribution in terms of the volume fractions of the constituents. The aerodynamic pressure is modeled using the quasi-steady first-order piston theory, while the acoustic load is assumed to be a white-Gaussian random pressure uniformly distributed over the panel surface. The effects of the volume fraction exponent, aerodynamic pressure, temperature rise, and sound pressure level on the nonlinear vibration behavior of a clamped FGM panel are studied.

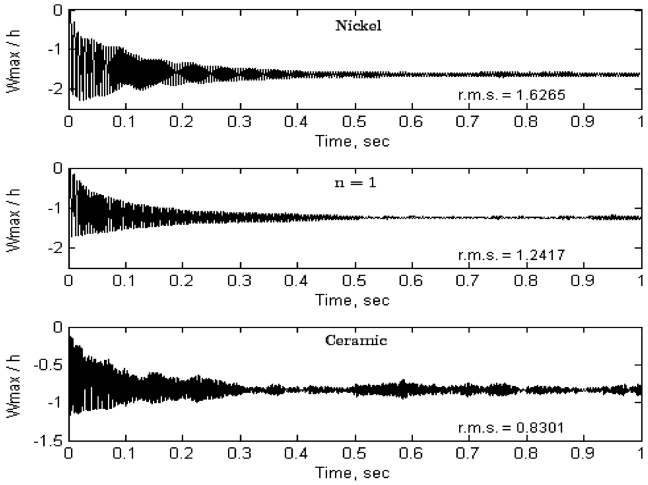


**Fig. 11 Time histories for an FGM panel at SPL = 110 dB, $\lambda = 0$, $\Delta T = 24°C$, and different volume fraction exponent values.**

The results showed that, at room temperature, the nickel panel has a better performance regarding the random acoustic response. But, at higher temperatures, it turns out to be a matter of compromise between having large thermal postbuckling deflections and hence deterioration in the flight performance, or having higher vibration amplitudes which can affect fatigue life performance. It is also noticed that decreasing the volume fraction results in a reduction in the flutter amplitude and a noticeable increase in the frequency of vibration. Moreover, it is found that the flutter motion frequently dominates the random acoustic response, but high sound pressure levels can affect the flutter behavior through increasing the flutter frequency and changing the type vibration to be nonharmonic or chaotic limit-cycle oscillations. Accordingly, overlooking the existence of acoustic noise can lead to fatigue failure. Finally, it is concluded that for a panel under aerodynamic, thermal, and random acoustic loads, the FGM panels are not always superior in performance compared to the metal panels.

## Acknowledgment

This work was supported by the BK21 program, Hanyang University, Seoul, South Korea. The authors wish to express their gratitude for this financial support.

## References


[1] Dowell, E. H., "A Review of the Aeroelastic Stability of Plates and Shells," *AIAA Journal*, Vol. 8, 1970, pp. 385–399. doi:10.2514/3.5680

[2] Reddy, J. N., "Analysis of Functionally Graded Plates," *International Journal for Numerical Methods in Engineering*, Vol. 47, 2000, pp. 663–684. doi:10.1002/(SICI)1097-0207(20000110/30)47:1/3<663::AID-NME787>3.0.CO;2-8

[3] El-Abbasi, N., and Meguid, S. A., "Finite Element Modeling of the Thermoelastic Behavior of Functionally Graded Plates and Shells," *International Journal of Computational Engineering Science*, Vol. 1, 2000, pp. 151–165. doi:10.1142/S1465876300000082

[4] Zenkour, A. M., "Generalized Shear Deformation Theory for Bending Analysis of Functionally Graded Plates," *Journal of Applied Mathematical Modeling*, Vol. 30, 2005, pp. 67–84.

[5] Dai, K. Y., Liu, G. R., Han, X., and Lim, K. M., "Thermomechanical Analysis of Functionally Graded Material (FGM) Plates Using Element-Free Galerkin Method," *Computers and Structures*, Vol. 83, 2005, pp. 1487–1502. doi:10.1016/j.compstruc.2004.09.020

[6] He, X. Q., Ng, T. Y., Sivashanker, S., and Liew, K. M., "Active Control of FGM Plates with Integrated Piezoelectric Sensors and Actuators," *International Journal of Solids and Structures*, Vol. 38, 2001, pp. 1641–1655. doi:10.1016/S0020-7683(00)00050-0

[7] Yang, J., Kitipornchai, J., and Liew, K. M., "Non-Linear Analysis of the Thermo-Electro-Mechanical Behavior of Shear Deformable FGM Plates with Piezoelectric Actuators," *International Journal for Numerical Methods in Engineering*, Vol. 59, 2004, pp. 1605–1632. doi:10.1002/nme.932

[8] Batra, R. C., and Jin, J., "Natural Frequencies of a Functionally Graded Anisotropic Rectangular Plate," *Journal of Sound and Vibration*, Vol. 282, 2005, pp. 509–516. doi:10.1016/j.jsv.2004.03.068

[9] Kim, Y. W., "Temperature Dependent Vibration Analysis of Functionally Graded Rectangular Plates," *Journal of Sound and Vibration*, Vol. 284, 2005, pp. 531–549. doi:10.1016/j.jsv.2004.06.043

[10] Prakash, T., and Ganapathi, M., "Supersonic Flutter Characteristics of Functionally Graded Flat Panels Including Thermal Effects," *Composite Structures*, Vol. 72, 2006, pp. 10–18. doi:10.1016/j.compstruct.2004.10.007

[11] Navazi, H. M., and Haddadpour, H., "Aero-Thermoelastic Stability of Functionally Graded Plates," *Composite Structures*, Vol. 80, 2007, pp. 580–587. doi:10.1016/j.compstruct.2006.07.014

[12] Haddadpour, H., Navazi, H. M., and Shaadmehri, F., "Nonlinear Oscillations of a Fluttering Functionally Graded Plate," *Composite Structures*, Vol. 79, 2007, pp. 242–250. doi:10.1016/j.compstruct.2006.01.006

[13] Ibrahim, H. H., Tawfik, M., and Al-Ajmi, M., "Aero-Thermo-Mechanical Characteristics of Functionally Graded Material Panels with Temperature-Dependent Material Properties," *Proceedings of the 8th International Congress of Fluid Dynamics and Propulsion (ICFDP8)*, American Society of Mechanical Engineers, Fairfield, NJ, ICFDP-EG-116, 2006.

[14] Ibrahim, H. H., Tawfik, M., and Al-Ajmi, M., "Non-Linear Panel Flutter For Temperature-Dependent Functionally Graded Material Panels," *Computational Mechanics*, Vol. 41, No. 2, 2008, pp. 325–334.

[15] Ibrahim, H. H., Tawfik, M., and Al-Ajmi, M., "Thermal Buckling and Nonlinear Flutter Behavior of Functionally Graded Material Panels," *Journal of Aircraft*, Vol. 44, No. 5, 2007, pp. 1610–1618. doi:10.2514/1.27866

[16] Sohn, K.-J., and Kim, J.-H., "Structural Stability of Functionally Graded Panels Subject to Aerothermal Loads," *Composite Structures*, Vol. 82, 2008, pp. 317–325. doi:10.1016/j.compstruct.2007.07.010

[17] Bogner, F. K., Fox, R. L., and Schmit, L. A., "The Generation of Inter-Element Compatible Stiffness and Mass Matrices by the Use of Interpolation Formulas," Wright–Patterson AFB, OH, AFFDL-TR-66-80, 1966, pp. 396–443.

[18] Dhainaut, J. M., Gou, X., Mei, C., Spottswood, S. M., and Wolfe, H. F., "Nonlinear Random Response of Panels in an Elevated Thermal-Acoustic Environment," *Journal of Aircraft*, Vol. 40, 2003, pp. 683–691. doi:10.2514/2.3146

[19] Xue, D. Y., "Finite Element Frequency Domain Solution of Nonlinear Panel Flutter with Temperature Effects and Fatigue Life Analysis," Ph.D. Dissertation, Old Dominion University, Mechanical Engineering Department, Norfolk, VA, 1991.

[20] Ibrahim, H. H., Tawfik, M., and Negm, H. M., "Thermo-Acoustic Random Response of Shape Memory Alloy Hybrid Composite Plates," *Journal of Aircraft*, Vol. 45, No. 3, 2008, pp. 962–970. doi:10.2514/1.32843

[21] Dowell, E. H., "Nonlinear Oscillation of a Fluttering Plate I," *AIAA Journal*, Vol. 4, No. 7, 1966, pp. 1267–1275. doi:10.2514/3.3658

[22] Bathe, K. J., *Finite Element Procedures*, Prentice–Hall, Inc., Englewood Cliffs, NJ, 1996.

[23] Yoo, H. H., "Dynamic Modeling of Flexible Bodies in Multibody Systems," Ph.D. Dissertation, Michigan University, Mechanical Engineering Department, Dearborn, MI, 1989.

[24] Touloukian, Y. S., *Thermophysical Properties of High Temperature Solid Materials*, McMillan, New York, 1967.